An emerging PB2-627 polymorphism increases the pandemic potential of avian influenza virus by breaking through ANP32 host restriction in mammalian and avian hosts

Yuxin Guo[1], Sicheng Shu[1], Yong Zhou[1], Wenjing Peng[1], Zhimin Jiang[1], Yudong Li[1], Tian Li[1], Fanshu Du[1], Linlin Wang[1], Xue Chen[1], Jinze Dong[1], Chuankuo Zhao[1], Maggie Haitian Wang[2,3], Yipeng Sun[1], Honglei Sun[1], Lu Lu[4], Paul Digard[4], Kin-Chow Chang[5], Hui-Ling Yen[6], Jinhua. Liu[1*], Juan Pu[1*]

Affiliations:

[1] National key laboratory of Veterinary public health security, Key Laboratory for Prevention and Control of Avian Influenza and Other Major Poultry Diseases, Ministry of Agriculture and Rural Affairs, College of Veterinary Medicine, China Agricultural University; Beijing 100193, P.R. China.

[2] Centre for Clinical Research and Biostatistics, JC School of Public Health and Primary Care, the Chinese University of Hong Kong, Hong Kong SAR, China.

[3] CUHK Shenzhen Research Institute, Shenzhen, 518172, China.

[4] The Roslin Institute, University of Edinburgh, Edinburgh, EH25 9RG, United Kingdom.

[5] School of Veterinary Medicine and Science, University of Nottingham, Sutton Bonington Campus, Loughborough, LE12 5RD, UK.

[6] School of Public Health, Li Ka Shing Faculty of Medicine, The University of Hong Kong, Hong Kong Special Administrative Region, 999077, China.

*Corresponding author. Email: Juan Pu: pujuan@cau.edu.cn; Jinhua Liu: ljh@cau.edu.cn.

Abstract

Alterations in the PB2-627 domain could substantially increase the risk of an avian influenza virus (AIV) pandemic. Here, we discovered a variant, PB2-627V, which combines the properties of avian-like PB2-627E and human-like PB2-627K. This variant not only maintains viral fitness in chickens but also facilitates the aerosol transmission of AIVs between ferrets. Mechanistically, PB2-627V utilizes both avian and human host protein ANP32A to support viral polymerase function. Therefore, this mutation overcomes the barrier between birds and humans, greatly enhancing the likelihood of AIVs infecting humans. The PB2-627V polymorphism has been found in birds, humans, and mammals worldwide across more than ten AIV subtypes. Given the escalating global spread of AIVs, it is crucial to closely monitor influenza viruses carrying PB2-627V to prevent a pandemic.

Introduction

Avian influenza viruses (AIVs) are critically important in the evolution of pandemic influenza viruses [1]. Adaptive changes in AIVs allow breakthrough infection in mammalian species through altering viral interactions with host-specific factors [2–4]. The current clade 2.3.4.4b highly pathogenic avian influenza (HPAI) H5Ny virus outbreaks have swept across continents, posing an unprecedented panzootic threat to birds, mammals, and public health [5] (https://www.who.int/news/item/12-07-2023-ongoing-avian-influenza-outbreaks-in-animals-pose-risk-to-humans). Other subtypes of AIVs have also been responsible for recurrent human infections [6]. For example, H7N7 [7], H7N9 [8,9], H10N8 [10], H5N6 [11], H10N3 [12] and H3N8 [13] viruses have caused over 1600 documented human cases [11]. Notably, most of these AIV subtypes possess internal (i.e. non-glycoprotein) genes that are derived from avian H9N2 viruses [8,11–13]. H9N2 virus is globally widespread in wild and domestic birds [14,15], and causes repeated human infections, especially since 2015. In these interspecies transmission events, critical adaptive mutations often occur on the PB2 protein of AIVs [12,16–19].

PB2 is one of three polymerase subunits of the influenza virus RNA-dependent RNA polymerase (RdRP), crucial for genome transcription and replication[20]. Specific amino acid changes have been identified in PB2 as key determinants of avian-to-mammalian adaptation, through its interaction with host acidic leucine-rich nuclear phosphoprotein 32 (ANP32) in avian and mammalian cells [21–24]. Their interactions exhibit host-species specificity[23]. PB2-627K in human influenza viruses interacts with human ANP32A and ANP32B (huANP32A and huANP32B) to support viral polymerase function [22]. On the other hand, PB2-627E in AIV can utilize avian ANP32A, but not huANP32A or huANP32B [22]. PB2-E627K amino acid substitution in AIVs promotes viral polymerase activity in mammalian cells by enhancing PB2 interaction with huANP32A and huANP32B [25]. Fortunately, the PB2-627K genotype is only frequently detected in AIVs isolated from human infections, and rarely detected in AIVs isolated from poultry or wild birds [26], greatly reducing the possibility of AIVs transmission to humans. In this study, we discovered an emerging PB2-627 polymorphism (PB2-627V) in diversified subtypes that increases the pandemic potential of AIVs by breaking through ANP32 host restriction in mammalian and avian hosts.

Results

PB2-627V prevalence in influenza virus isolates from avian and mammalian species

Given the crucial role of PB2 residue 627 in host adaptation, we analyzed a total of 42,297 influenza PB2 sequences worldwide (excluding human H3N2 and H1N1pdm09 viruses) for polymorphisms at this position. We found that the number of sequences with PB2-627V rapidly increased after 2016 (Fig. 1A). Among these viruses with PB2-627V, 71.3% were isolated from

avian species, 14.7% were from humans, 14.0% were from other mammalian hosts (such as fox, swine, tiger, and mink) and environment (Fig. 1A, B and table S1). In geographical distribution, 61.7% of the viruses were isolated in China, with the remaining (38.3%) found in the Middle East, Germany, Mexico, Canada, Italy, Spain, Russia, America, Denmark, and Belgium (Fig. 1A, B, and table S1). In terms of subtype distribution, 64.5% of PB2-627V variants were detected in H9N2 viruses, 9.9% in H7N9 and 9.1% in H5N6 viruses; the remaining 16.5% were in various other subtypes: H1N1, H1N2, H3N2, H3N8, H5N1, H5N2, H6N6, H7N1, and H10N3 (Fig. 1, A and B, and table S1). Notably, PB2-627V has also been identified in clade 2.3.4.4b H5N1 viruses isolated from wild birds and red foxes (Fig. 1, A and B, and table S1).

In phylogenetic analysis, recent PB2-627V sequences mainly belong to a major group that includes most human and avian isolates from multiple subtypes (H9N2, H7N9, H5N6, H3N8, H10N3, and H5N1 viruses) (Fig. 1B). For H9N2 subtype, PB2 gene showed the evolution of a PB2-627V cluster (fig. S1A). Ancestral host reconstruction on time-scaled phylogeny indicated that chicken isolates are the origin of human isolates within this cluster (fig. S1B). Notably, PB2-627V of H9N2 is more frequently detected in humans than avian isolates from 2016-2022 (Fig. 1C). Similarly, there was a dramatic increase in PB2-627V detection in avian and human hosts for the H7N9, H5N6, and H3N8 subtypes after 2016 (fig. S2). Thus, it appears that PB2-627V has achieved better adaptability in poultry populations and its emerging prevalence both in avian and humans suggests functional significance across various host species.

PB2-627V promotes polymerase activity of H9N2 AIV in human and chicken cells by utilizing ANP32 proteins of both host species

To evaluate the functionality of PB2-627V, we used a previously identified chicken H9N2 isolate A/chicken/Hubei-m0530/2017 (referred to as 17/H9N2^{627E}) with PB2-627E as the backbone, and introduced the PB2-E627V and PB2-E627K changes. Although PB2-627V and -627K are found in other natural chicken isolates, this approach allowed the dissection of the function of this single mutation. A dual-luciferase assay system was used to compare viral polymerase activities conferred by PB2-627E, V, and K in avian DF-1 cells and human 293T cells at 33°C and 37°C, respectively, mimicking the temperature of human upper and lower respiratory tract [27]. In DF-1 cells, 17/H9N2^{627E}, 17/H9N2^{627V}, and 17/H9N2^{627K} showed comparable polymerase levels at 33°C and 37°C (Fig. 1D). However, a 23.6-fold (±2.6) increase in polymerase activity at 33°C, and an 11.8-fold (±0.6) increase at 37°C were found with 17/H9N2^{627V} in 293T cells compared with 17/H9N2^{627E} ($p < 0.001$); 17/H9N2^{627K} exhibited a 9.3-fold (±2.6) increase in polymerase activity at 33°C and a 20.2-fold (±0.4) increase at 37°C ($p < 0.001$) relative to 17/H9N2^{627E} (Fig. 1E). Accordingly, in avian DF1 cells, PB2-627V demonstrated more robust

83 viral transcriptional and replication functions than PB2-627K, while in human A549 cells, it
84 surpassed PB2-627E (fig. S3, A and B).
85 Viral polymerase activity was further examined in ANP32A and ANP32B double-knockout
86 293T (DKO) cells over-expressing chicken- or human-ANP32 protein(s) [25]. As expected,
87 polymerase activities of all 3 viruses (17/H9N2^{627E}, 17/H9N2^{627V}, and 17/H9N2^{627K}) in control
88 DKO cells were significantly lower than those in the wild type 293T cells (fig. S3C). Polymerase
89 activity of 17/H9N2^{627E} in the DKO cells was significantly enhanced in the presence of chicken
90 ANP32A (chANP32A) at both 33°C and 37°C ($p < 0.05$) (Fig. 1F). With 17/H9N2^{627V}, chANP32A
91 in DKO cells significantly enhanced the polymerase activity at both 33°C and 37°C ($p < 0.05$),
92 and huANP32A significantly enhanced polymerase activity only at 37°C ($p < 0.001$) (Fig. 1F).
93 With 17/H9N2^{627K}, expression of chANP32A in DKO cells significantly enhanced viral
94 polymerase activity only at 37°C ($p < 0.001$), and huANP32A and huANP32B significantly
95 enhanced the polymerase activity at both 33°C and 37°C ($p < 0.001$) (Fig. 1F).
96 ANP32 interface with PB2 at the 627-domain by electrostatic and hydrophobic interactions
97 [28]. PB2-627K (lysine) has a positive charge and PB2-627E (glutamic acid) has a negative charge.
98 Modeling the surface electrostatic potential predicted that valine at PB2-627 confers a neutral state
99 (Fig. 1G), which could permit the PB2 protein to interact sufficiently with avian and human
100 ANP32A proteins to promote viral polymerase activity in avian and human cells. In summary,
101 these findings indicate that PB2-627V can utilize chicken and human ANP32A in the respective
102 species of cells to facilitate viral polymerase activity.

103 **PB2-627V in H9N2 virus maintains efficient replication in chickens and facilitates**
104 **replication in human cells and mice**

105 Next, viruses with the three PB2 627 polymorphisms were rescued on the background of the
106 17/H9N2 virus. The replication kinetics of these 17/H9N2^{627E}, 17/H9N2^{627V}, and 17/H9N2^{627K}
107 viruses were assessed in avian CEF cells; no significant differences in replication were found
108 between viruses ($p > 0.05$) (Fig. 2A). Chickens individually inoculated with 10^6 EID_{50} of each
109 virus showed no mortality (fig. S4A) and no apparent clinical signs. Viral loads detected from
110 oropharyngeal swabs of 17/H9N2^{627V} and 17/H9N2^{627E} inoculated chickens were significantly
111 higher than those infected with 17/H9N2^{627K} at 6 and/or 8 dpi ($p < 0.05$) (Fig. 2B). The three
112 viruses replicated to comparable titers in the turbinates at 3 dpi, but 17/H9N2^{627V} replicated to
113 higher titers than 17/H9N2^{627K} in the lungs ($p < 0.05$) (Fig. 2C). Histopathological examination of
114 chicken lungs at 3 dpi indicate that all viruses induced inflammatory responses, with more
115 hemorrhage noted in 17/H9N2^{627V} infected lungs (Fig. 2D). These findings indicate that PB2-627V
116 and PB2-627E replicated comparably well in chickens.

117 In infected human A549 cells, virus titers of 17/H9N2^{627V} and 17/H9N2^{627K} were significantly
118 higher than that of 17/H9N2^{627E} from 12 to 48 hpi ($p < 0.001$); there was no significant difference
119 between 17/H9N2^{627V} and 17/H9N2^{627K} ($p > 0.05$) (Fig. 2E). Mice inoculated with 17/H9N2^{627E},
120 17/H9N2^{627V}, or 17/H9N2^{627K} virus, showed no obvious clinical signs, as in infected chickens (Fig.
121 2F and fig. S4B). Higher virus loads were detected in the nasal turbinates and lungs of mice
122 infected with 17/H9N2^{627V} and 17/H9N2^{627K} at 3 dpi than those with 17/H9N2^{627E} ($p < 0.001$);
123 there was no significant difference in virus titers between the 17/H9N2^{627V} and 17/H9N2^{627K}
124 groups ($p > 0.05$) (Fig. 2G). Likewise, 17/H9N2^{627V} and 17/H9N2^{627K} viruses produced more viral
125 NP protein-positive cells in the lung than in corresponding 17/H9N2^{627E} infected mice (Fig. 2H).
126 Thus, the infectivity of PB2-627V H9N2 virus in human cells and mice is similar to that of PB2-
127 627K virus.

128 **PB2-627V confers aerosol transmission of H9N2 virus in ferrets**

129 Transmissibility of influenza viruses between ferrets is an indicator of potential epidemic or
130 pandemic risk. Direct contact (DC) and respiratory droplet (RD) transmission tests of the
131 17/H9N2^{627E}, 17/H9N2^{627V}, and 17/H9N2^{627K} viruses were performed in ferrets. All viruses
132 infected the directly infected donor animals, as assessed by virus titers in nasal washes (Fig. 3, A-
133 C, and table S2). 17/H9N2^{627V} and 17/H9N2^{627K} viruses were transmitted to all DC ferrets and all
134 RD ferrets, but 17/H9N2^{627E} was only transmitted to DC groups. Transmission by RD in the
135 17/H9N2^{627V} group took place around 2 days later than in the 17/H9N2^{627K} group (Fig. 3, A-C).
136 Areas under the curve (AUC), based on virus titers over time in the nasal washes, were determined
137 to compare total viral shedding during infection (Fig. 3D and table S3). In donor ferrets, virus
138 production was comparable between the three viruses. In DC ferrets, 17/H9N2^{627V} virus output
139 (AUC = 18.13 ± 3.69) was slightly higher than that of 17/H9N2^{627E} virus (14.13 ± 3.01, $p = 0.19$)
140 and 17/H9N2^{627K} virus (16.25 ± 1.27, $p = 0.68$). In RD ferrets, 17/H9N2^{627V} virus output (AUC =
141 11.75 ± 2.88) was slightly lower than that of 17/H9N2^{627K} virus (15.42 ± 1.60, $p = 0.25$) (Fig. 3D
142 and table S3). Thus, in contrast to PB2-627E, PB2-627V promotes aerosol transmissibility of
143 H9N2 virus in ferrets.

144 To monitor any polymorphic changes at residue PB2-627 during virus infection and
145 transmission, next-generation sequencing was performed on nasal wash samples from each ferret
146 at the first and the last time points of positive virus detection. In 17/H9N2^{627E} groups, 627E
147 remained the dominant genotype in the donors and DC ferrets (Fig. 3E). In the donor groups of
148 17/H9N2^{627V} and 17/H9N2^{627K}, 627V and 627K were the corresponding dominant genotypes. In
149 the DC and RD transmission groups of 17/H9N2^{627V} and 17/H9N2^{627K}, polymorphisms at PB2-
150 627 during infection were more noticeable, but at the last detection time point of each RD group,

151 corresponding 627V and 627K returned to their earlier dominance (Fig. 3, F and G). These results
152 suggest that residue PB2-627V stably confers aerosol transmission of H9N2 virus in ferrets.

153 **PB2-627V has the potential for sustained prevalence in poultry**

154 17/H9N2^{627E}, 17/H9N2^{627V}, and 17/H9N2^{627K} H9N2 viruses were serially passaged in
155 chickens to assess the potential for sustained prevalence of PB2-627V in poultry. Chickens were
156 directly infected with each virus (Passage 1, P1) and subsequently (P2 - P5) passaged through
157 contact transmission (Fig. 4A). All viruses were successfully passaged from P1 to P5. We then
158 performed next-generation sequencing of whole viral genomes from RNA isolated from the lungs
159 of the P5 chickens. Mutations above 1% threshold were identified as intra-host single nucleotide
160 variants (iSNVs) [29,30]. Overall, most iSNVs were detected at low frequency and there were no
161 significant differences between the 3 groups (Fig. 4B). Notably, variant frequency at residue PB2-
162 627 was below the 1% threshold in all P5 chicken samples (Fig. 4C). At the amino-acid level, two
163 variant residues (PA-D529N, NP-T211D) occurred at a high frequency (>10%) in the 17/H9N2^{627K}
164 group, but no high-frequency variant residues were detected in 17/H9N2^{627E} and 17/H9N2^{627V}
165 groups (Fig. 4D), suggesting that compared to PB2-627E and PB2-627V, PB2-627K required other
166 cooperative mutations in RNP genes for transmission in chickens. Taken together, PB2-627V
167 showed a high potential for sustained prevalence in chickens.

168 **PB2-627V confers dual ability to replicate in chickens and mice to avian H7N9 and H3N8**
169 **viruses**

170 We determined if the dual host adaptability of PB2-627V, detected at high frequency in the
171 H9N2 virus, is transferrable to other AIV subtypes. H7N9 and H3N8 viruses possess the PB2 gene
172 and other internal genes derived from the H9N2 viruses [9,31]. The natural mutations PB2-E627V
173 and PB2-E627K were separately introduced into the LPAI H7N9 (A/chicken/China/0606-12/2017,
174 referred as 17/H7N9^{627E}) and H3N8 (A/chicken/Anhui/FE12/2022, referred as 22/H3N8^{627E}) [32]
175 viruses. The resulting PB2-627V, PB2-627K, and PB2-627E viruses were assessed for replication
176 and pathogenicity in chickens and mice.

177 In chickens, introduction of PB2-E627V or PB2-E627K mutation into 17/H7N9 and 22/H3N8
178 viruses did not significantly affect replication or pathogenicity relative to their PB2-627E
179 counterparts (Fig. 5, A-E), although the replication of 17/H7N9^{627V} in chicken lungs was
180 significantly higher than that of 17/H7N9^{627K} ($p<0.05$) (Fig. 5B). Thus, PB2-E627V had little
181 effect on virus replication and pathogenicity in chickens (Fig. 5, A-E, and fig. S5A). In mice, both
182 PB2-E627V and PB2-E627K changes in 17/H7N9 and 22/H3N8 viruses led to virus loads in the
183 nasal turbinates and lungs, weight loss, and mortality ($p<0.01$) (Fig. 5, F-K). Murine lungs at 3 dpi.
184 with subtypes housing PB2-627V showed more severe pathology than those with PB2-627E (Fig.

185 5L and fig. S5B). In summary, PB2-E627V significantly increases pathology and replication of
186 H7N9 and H3N8 virus subtypes in mice and maintains their replication fitness in chickens.

187 **Discussion**

188 Here, we identified PB2-627V as an emerging variant in AIVs with significant zoonotic and
189 pandemic potential. We observed that PB2-627V enhances the polymerase activity of H9N2 AIV
190 in both human and chicken cells by utilizing ANP32A proteins from both species, thereby
191 overcoming the restriction imposed by human ANP32 on AIVs carrying PB2-627E and exhibiting
192 properties similar to those with PB2-627K. PB2-627V in H9N2 virus maintains efficient
193 replication in chickens, facilitates virus replication in mice, and confers aerosol transmission in
194 ferrets. Furthermore, PB2-627V is stably maintained in passages through chickens and also
195 conferred the dual ability to replicate in chickens and mice to avian H7N9 and H3N8 subtype
196 viruses. Thus, the increased prevalence of this dual adaptive mutation of PB2-E627V in poultry
197 greatly increases the chances of AIVs infecting humans. In addition, the wide distribution of this
198 mutation in multiple subtypes, hosts, and countries poses global public health risks.

199 Clinical data and phylogenetic analysis revealed that residue PB2-627V originated in chicken
200 influenza viruses (likely the H9N2 subtype) and was subsequently transmitted to humans. The
201 prevalence of PB2-627V in AIVs is on the rise, particularly within the H9N2 subtype, and PB2-
202 627V is also found in other subtypes such as H7N9, H5N6, H3N8, and H10N3, which contain
203 reassorted internal genes derived from H9N2 [8,11–13]. Serial passage studies in chickens further
204 indicate that additional mutations occurred in the polymerase protein after the passage of H9N2
205 viruses with the PB2-E627K. However, H9N2 viruses with PB2-627E and -627V did not produce
206 further mutations. This may be due to the PB2-627K mutation still having defects in transmission
207 in chickens and requiring further adaptation. This could explain why PB2-627K is very rare in
208 avian isolates. The PB2-E627K mutation usually takes place in infected humans [33]. Conversely,
209 PB2-627V appears to be a product of evolution in H9N2 virus and has a high potential for long-
210 term prevalence in poultry populations, posing an increasing likelihood of viral transmission to
211 humans.

212 Cellular ANP32 proteins specifically support influenza virus genome replication. ANP32A
213 can bridge PB2 dimers and form extensive contacts with two polymerases to maintain a dimeric
214 assembly [22,34]. The C-terminal low complexity acidic region ($ANP32A^{LCAR}$) inserts between two
215 PB2-627 domains of the polymerase dimer. Human $ANP32A^{LCAR}$ contains only acidic amino acid
216 residues. Thus, with human ANP32A, basic or uncharged residues (such as lysine, K or valine, V)
217 are preferred in the PB2-627 domain to acidic amino acids (such as glutamic acid, E) [21,22]. In avian
218 cells, the additional 33 amino acids in $chANP32A^{LCAR}$ allow AIVs carrying PB2-627E to
219 effectively utilize chANP32A in avian cells [23,35]. Indeed, in the context of H9N2, we found that

220 the polymerase activity of PB2-627V in avian cells is comparable to PB2-627E, and in human
221 cells is comparable to PB2-627K which suggests that the nonpolar neutral amino acid of PB2-
222 627V has the dual ability to interact with avian ANP32A and human ANP32A in different host
223 cells. It is noteworthy that, when the PB2-627 site is changed from E to V, the virus can not only
224 undergo contact transmission in ferrets but also undertake effective aerosol transmission, similar
225 to that of the 17/H9N2^{627K} variant. In addition, PB2-627V can be maintained in ferret post-
226 infection, during contact and aerosol transmission. Thus, these features suggest that the dual
227 adaptive PB2-627V AIVs reduce the host barrier between avians and humans.
228 The PB2-E627V has been identified in H5N1 viruses where it was shown to increase viral
229 replication in mammalian cells and virulence in mice [36], while in the background of a laboratory
230 strain of H1N1 (PR8), it reduced viral replication in mammalian cells compared with PB2-627K
231 [37]. However, because the PB2-627V variant was rarely found in natural influenza isolates at that
232 time (before 2015), it did not attract much attention. In H9N2 AIVs, PB2-627V variants appeared
233 in the Middle East from 2000 to 2015 but were not stably maintained. The genotype of Middle
234 East H9N2 viruses was very different from the G57 lineage [8] H9N2 virus prevalent in China and
235 studied here [38,39]. Under experimental conditions, PB2-627V in the Middle East H9N2 virus needs
236 to operate in concert with PB2-E543D, PB2-A655V and PB2-K526R to enhance viral replication
237 in mammals [38]. Numerous adaptive mutations have recently been identified in the G57 H9N2 virus,
238 including PB2-292, PB2-588, PA-356, M1-37 and HA-226 [15,40,41], in avian and human isolates [42–
239 45]. It is plausible that one or more of these adaptive changes in the G57 genotype exert epistatic
240 effects to induce the emergence of the stable PB2-627V residue, but this remains to be tested.
241 Collectively, our results suggest that the recent evolved variant PB2-E627V combines the
242 characteristics of avian-like PB2-627E and human-like PB2-627K. It exhibits a crucial dual-
243 adaptation that can effectively infect and transmit in both avian and mammalian hosts, thereby
244 overcoming the interspecific barrier between birds and humans. The presence of PB2-627V in
245 multiple subtypes of AIVs undoubtedly escalates the risk of an avian influenza virus pandemic.
246 We therefore recommend considering PB2-627V as a new molecular marker to assess the
247 pandemic potential of AIVs.
248

References and Notes

1. Krammer, F. *et al.* Influenza. *Nat Rev Dis Primers* 4, 3 (2018).
2. Amat, J. A. R. *et al.* Long-term adaptation following influenza A virus host shifts results in increased within-host viral fitness due to higher replication rates, broader dissemination within the respiratory epithelium and reduced tissue damage. *PLoS Pathog* 17, e1010174 (2021).
3. Su, W. *et al.* Ancestral sequence reconstruction pinpoints adaptations that enable avian influenza virus transmission in pigs. *Nat Microbiol* 6, 1455–1465 (2021).
4. Wang, J. & Samaan, M. Tool for Influenza Pandemic Risk Assessment - version 2. 65.
5. European Food Safety Authority, European Centre for Disease Prevention and Control, European Union Reference Laboratory for Avian Influenza *et al.* Avian influenza overview April – June 2023. *EFS2* 21, (2023).
6. Bi, Y., Li, J. & Shi, W. The time is now: a call to contain H9N2 avian influenza viruses. *The Lancet Microbe* S2666524722002324 (2022) doi:10.1016/s2666-5247(22)00232-4.
7. Koopmans, M. *et al.* Transmission of H7N7 avian influenza A virus to human beings during a large outbreak in commercial poultry farms in the Netherlands. *Lancet* 363, 587–593 (2004).
8. Pu, J. *et al.* Evolution of the H9N2 influenza genotype that facilitated the genesis of the novel H7N9 virus. *P Natl Acad Sci USA* 112, 548–553 (2015).
9. Pu, J. *et al.* Reassortment with Dominant Chicken H9N2 Influenza Virus Contributed to the Fifth H7N9 Virus Human Epidemic. *J Virol* 95, e01578-20 (2021).
10. Chen, H. *et al.* Clinical and epidemiological characteristics of a fatal case of avian influenza A H10N8 virus infection: a descriptive study. *Lancet* 383, 714–721 (2014).
11. Bi, Y. *et al.* Genesis, Evolution and Prevalence of H5N6 Avian Influenza Viruses in China. *Cell Host & Microbe* 20, 810–821 (2016).
12. Qi, X. *et al.* Human infection with an avian-origin influenza A(H10N3) virus. *N Engl J Med* 386, 1087–1088 (2022).
13. Bao, P. *et al.* Human infection with a reassortment avian influenza A H3N8 virus: an epidemiological investigation study. *Nat Commun* 13, 6817 (2022).
14. Li, C. *et al.* Evolution of H9N2 influenza viruses from domestic poultry in Mainland China. *Virology* 340, 70–83 (2005).
15. Peacock, T. P., James, J., Sealy, J. E. & Iqbal, M. A global perspective on H9N2 avian influenza virus. *Viruses* 11, 620 (2019).
16. Elgendy, E. M. *et al.* Double mutations in the H9N2 avian influenza virus PB2 gene act cooperatively to increase viral host adaptation and replication for human infections. *Journal of General Virology* 102, (2021).
17. Gao, Y. *et al.* Identification of amino acids in HA and PB2 critical for the transmission of H5N1 avian influenza viruses in a mammalian host. *PLoS Pathog* 5, e1000709 (2009).
18. Arai, Y. *et al.* Multiple polymerase gene mutations for human adaptation occurring in Asian H5N1 influenza virus clinical isolates. *Sci Rep* 8, 13066 (2018).
19. Zaraket, H. *et al.* Mammalian adaptation of influenza A(H7N9) virus is limited by a narrow genetic bottleneck. *Nat Commun* 6, 6553 (2015).
20. Long, J. S., Mistry, B., Haslam, S. M. & Barclay, W. S. Host and viral determinants of influenza A virus species specificity. *Nat Rev Microbiol* 17, 67–81 (2019).
21. Camacho-Zarco, A. R. *et al.* Molecular basis of host-adaptation interactions between influenza virus polymerase PB2 subunit and ANP32A. *Nat Commun* 11, 3656 (2020).
22. Carrique, L. *et al.* Host ANP32A mediates the assembly of the influenza virus replicase. *Nature* 587, 638–643 (2020).

295 23. Long, J. S. *et al.* Species difference in ANP32A underlies influenza A virus polymerase host
296 restriction. *Nature* 529, 101–104 (2016).
297 24. Subbarao, E. K., London, W. & Murphy, B. R. A single amino acid in the PB2 gene of influenza
298 A virus is a determinant of host range. *J Virol* 67, 1761–1764 (1993).
299 25. Zhang, H. *et al.* Fundamental contribution and host range determination of ANP32A and ANP32B
300 in influenza A virus polymerase activity. *J Virol* 93, e00174-19 (2019).
301 26. Briggs, K. & Kapczynski, D. R. Comparative analysis of PB2 residue 627E/K/V in H5 subtypes
302 of avian influenza viruses isolated from birds and mammals. *Frontiers in Veterinary Science* 10,
303 (2023).
304 27. Hatta, M. *et al.* Growth of H5N1 influenza A viruses in the upper respiratory tracts of mice. *PLoS*
305 *Pathog* 3, e133 (2007).
306 28. Mistry, B. *et al.* Elucidating the Interactions between Influenza Virus Polymerase and Host Factor
307 ANP32A. *J Virol* 94, e01353-19 (2020).
308 29. Braun, K. M. *et al.* Transmission of SARS-CoV-2 in domestic cats imposes a narrow bottleneck.
309 *PLoS Pathog* 17, e1009373 (2021).
310 30. Moncla, L. H. *et al.* Quantifying within-host diversity of H5N1 influenza viruses in humans and
311 poultry in Cambodia. *PLoS Pathog* 16, e1008191 (2020).
312 31. Yang, R. *et al.* Human infection of avian influenza a H3N8 virus and the viral origins: a descriptive
313 study. *The Lancet Microbe* 3, e824–e834 (2022).
314 32. Sun, H. *et al.* Airborne transmission of human-isolated avian H3N8 influenza virus between ferrets.
315 *Cell* 0, (2023).
316 33. Liu, W. J. *et al.* Dynamic PB2-E627K substitution of influenza H7N9 virus indicates the in vivo
317 genetic tuning and rapid host adaptation. 8 doi:10.1073/pnas.2013267117.
318 34. Zhu, Z., Fodor, E. & Keown, J. R. A structural understanding of influenza virus genome replication.
319 *Trends in Microbiology* 31, 308–319 (2023).
320 35. Baker, S. F., Ledwith, M. P. & Mehle, A. Differential splicing of ANP32A in birds alters its ability
321 to stimulate rna synthesis by restricted influenza polymerase. *Cell Rep* 24, 2581-2588.e4 (2018).
322 36. Taft, A. S. *et al.* Identification of mammalian-adapting mutations in the polymerase complex of
323 an avian H5N1 influenza virus. *Nature Communications* 6, (2015).
324 37. Chin, A. W. H. *et al.* Influenza A viruses with different amino acid residues at PB2-627 display
325 distinct replication properties in vitro and in vivo: revealing the sequence plasticity of PB2-627
326 position. *Virology* 0, 545–555 (2014).
327 38. Arai, Y. *et al.* PB2 mutations arising during H9N2 influenza evolution in the Middle East confer
328 enhanced replication and growth in mammals. *PLoS Pathog* 15, e1007919 (2019).
329 39. Li, X. *et al.* Genetics, receptor binding property, and transmissibility in mammals of naturally
330 isolated H9N2 avian influenza viruses. *PLoS Pathog* 10, e1004508 (2014).
331 40. Carnaccini, S. & Perez, D. R. H9 influenza viruses: an emerging challenge. *Cold Spring Harb*
332 *Perspect Med* 10, a038588 (2020).
333 41. Sun, X., Belser, J. A. & Maines, T. R. Adaptation of H9N2 influenza viruses to mammalian hosts:
334 a review of molecular markers. *Viruses* 12, 541 (2020).
335 42. Sun, Y. *et al.* Genotypic evolution and antigenic drift of H9N2 influenza viruses in China from
336 1994 to 2008. *Vet Microbiol* 146, 215–225 (2010).
337 43. Xu, G. *et al.* Prevailing PA mutation K356R in avian influenza H9N2 virus increases mammalian
338 replication and pathogenicity. *Journal of Virology* 90, 8105–8114 (2016).
339 44. Gao, W. *et al.* Prevailing I292V PB2 mutation in avian influenza H9N2 virus increases viral
340 polymerase function and attenuates IFN-β induction in human cells. *J Gen Virol* 100, 1273–1281
341 (2019).

342 45. Xiao, C. *et al.* PB2-588 V promotes the mammalian adaptation of H10N8, H7N9 and H9N2 avian
343 influenza viruses. *Sci Rep-UK* 6, 19474 (2016).
344 46. Edgar, R. C. MUSCLE: a multiple sequence alignment method with reduced time and space
345 complexity. *BMC Bioinformatics* 5, 113 (2004).
346 47. Miller, M. A., Pfeiffer, W. & Schwartz, T. Creating the cipres science gateway for inference of
347 large phylogenetic trees. in *2010 Gateway Computing Environments Workshop (GCE)* 1–8 (2010).
348 doi:10.1109/gce.2010.5676129.
349 48. Chen, C. *et al.* TBtools-II: A "one for all, all for one" bioinformatics platform for biological big-
350 data mining. *Molecular Plant* 16, 1733–1742 (2023).
351 49. Su, Y. C. F. *et al.* Phylodynamics of H1N1/2009 influenza reveals the transition from host
352 adaptation to immune-driven selection. *Nat Commun* 6, 7952 (2015).
353 50. Hernandez, R. & Brown, D. T. Growth and maintenance of chick embryo fibroblasts (CEF). *Curr*
354 *Protoc Microbiol* Appendix 4, 4I (2010).
355 51. Zhang, P. *et al.* A novel genotype H9N2 influenza virus possessing human H5N1 internal genomes
356 has been circulating in poultry in eastern china since 1998. *J Virol* 83, 8428–8438 (2009).
357 52. Belser, J. A. *et al.* A guide for the use of the ferret model for influenza virus infection. *The*
358 *American Journal of Pathology* 190, 11–24 (2020).
359
360

Acknowledgments

We thank the Global Initiative on Sharing Avian Influenza Data (GISAID) for sharing the influenza virus sequence data used in this study. We are grateful to Xiaojun Wang (Harbin Veterinary Research Institute, China) for providing the DKO cells, Shangang Jia (China Agricultural University, China) for helpful suggestions on data analysis, and Nianzhi Zhang (China Agricultural University, China) for constructive suggestions on structure analysis. We thank BioRender (biorender.com) for assisting with graphics.

Funding

National Key Research and Development Program of China 2022YFF0802403 (JP)

National Key Research and Development Program of China 2021YFD1800202 (JP)

National Natural Science Foundation of China 32192450 to (JL)

National Natural Science Foundation of China 32102661 (ZJ)

UK Biotechnology and Biological Sciences Research Council BBS/E/D/20002173 (PD and LL)

Author contributions

Research designing: JP, YG

Data collection and analysis: YG, YZ, YL

Experiment: YG, TL, LW, XC, JD, CZ, FD

Funding acquisition: JP, JL, ZJ, PD, LL

Writing – original draft: YG, JP

Writing – review & editing: JL, HLY, LL, PD, KCC, MHW, HS, YS, ZJ, FD

Competing interests

Authors declare that they have no competing interests.

Data and materials availability

Genetic variation data of H9N2 viruses during passage in chickens are available at Mendeley data (DOI: 10.17632/zpvwwj59kx.1). All other data supporting the findings of this study are available w in the main text or the supplementary materials.

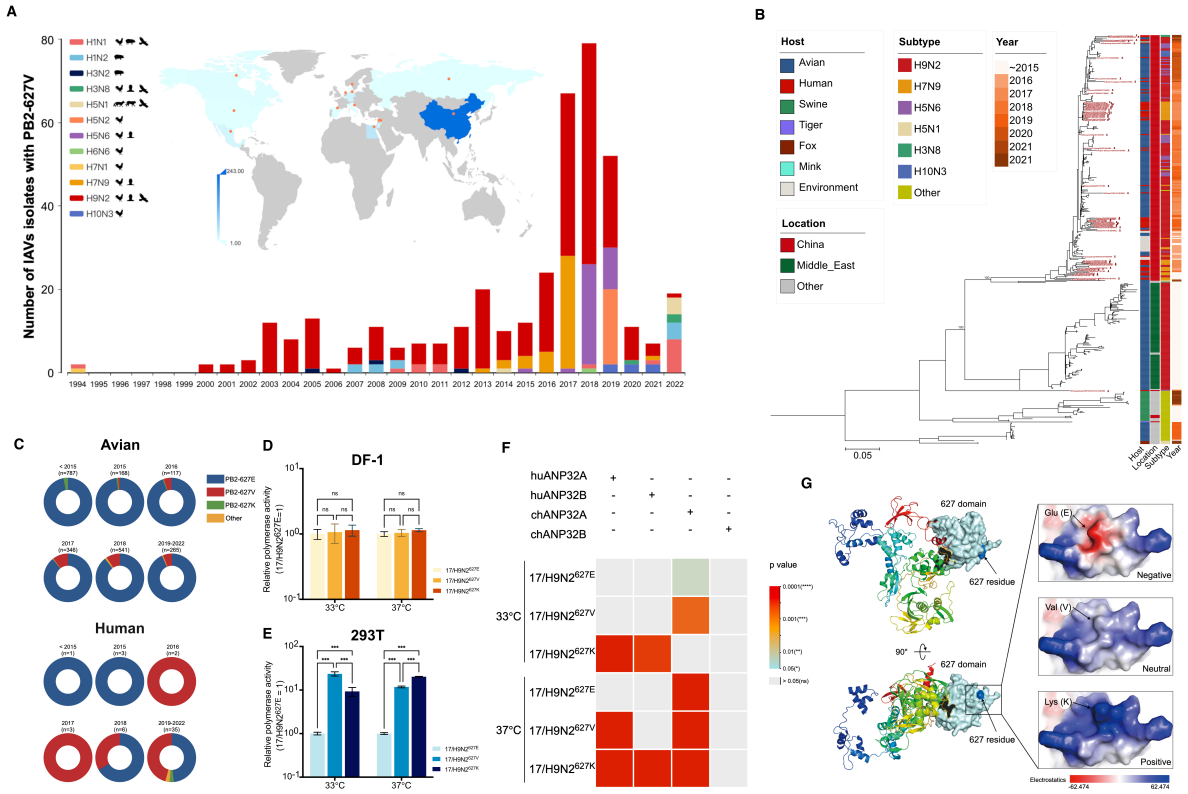

Fig. 1 Emergence and cross-host species function of PB2-627V. (**A**). The global prevalence of PB2-627V in influenza A viruses (IAVs) (excluding human H3N2 and H1N1pdm09 viruses) during 1994-2022. Bars show the number of isolates by subtype and host, while a world map displays the isolate's number by location. (**B**). Phylogenetic tree of PB2 genes with the residue 627V collected worldwide during 1994-2022 (n=394). Human isolates' names are in red. (**C**). Amino acid polymorphisms of the PB2-627 residue in avian and human-derived H9N2 viruses isolated in China. All sequence data were collected from the GISAID database**.** (**D-E**). Relative polymerase activities at 33°C or 37°C. DF-1 cells **(D)** and 293T cells **(E)** were transfected with firefly minigenome reporter, renilla expression control, and polymerase (PB2, PB1, PA, and NP) of 17/H9N2^{627E}, 17/H9N2^{627V}, or 17/H9N2^{627K}. Cells were incubated for 24 hours and the luciferase activities, normalized to corresponding renilla luciferase activity, are presented relative to 17/H9N2^{627E} (set as 1). Each data point is the mean ± SD of three independent experiments (one-way ANOVA). **(F).** Heat map shows p-values of polymerase activities in DKO cells overexpressing ANP32 proteins. chANP32A, chANP32B, huANP32A, huANP32B, or empty vector was transfected into DKO cells, incubated at 33°C and 37°C for 24 hours, and assayed the luciferase activity. Statistical significance was based on one-way ANOVA and subsequent Dunnett's test, compared with the corresponding value of empty vector (ns, not significant; *,

408 p<0.05; **, p<0.01; ***, p<0.001). (**G).** Impact of amino acids at the PB2-627 position on the
409 surface charge of the PB2 protein. Red (negative) and blue (positive) proteins are shown.
410

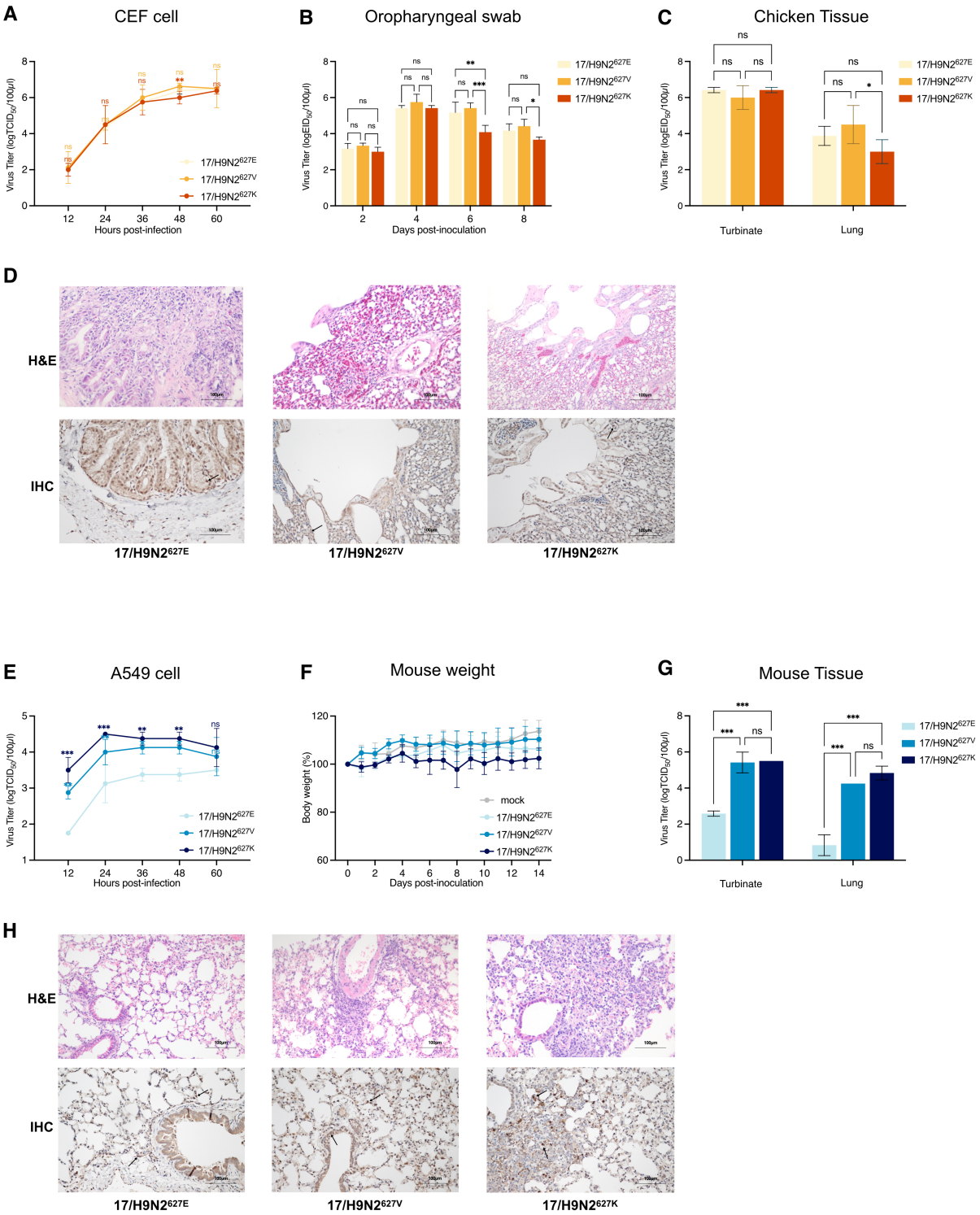

Fig. 2. PB2-627V conferred dual adaptability to H9N2 virus to replicate in avian and mammalian species. (**A**). CEF cells were infected with indicated viruses at 0.01 MOI and virus titers were determined at indicated times post-infection by $TCID_{50}$ assays. (**B-D**). Groups of 6 chickens were i.n. infected with indicated viruses at 10^6 EID_{50}, three chickens from each group

were used to determine the viral titers (**B**) from oropharyngeal samplings at 2, 4, 6, and 8 dpi. Another three chickens from each group were euthanized at 3 dpi. Virus titers (**C**) of the turbinates and lungs were determined. Representative histopathological findings (**D**) in the lungs of infected mice. Lung sections were stained with H&E (upper) and by IHC against influenza viral NP antigen (lower). Scale bars, 100 mm. (**E).** A549 cells were infected with indicated viruses at 0.1 MOI and virus titers were determined by $TCID_{50}$ assays at indicated times post-infection. (**F-H).** Groups of 8 mice were infected with the indicated virus at doses of 10^6 $TCID_{50}$. Five mice of each group were monitored for body weight changes (**F**) over 14 days. Additional three mice from each group at 3 dpi were euthanized. Virus titers (**G**) in the turbinates and lungs were determined by $TCID_{50}$ assays. Representative histopathological findings (**H**) in the lungs of infected mice. Lung sections were stained with H&E (upper) and by IHC against influenza viral NP antigen (lower). Scale bars, 100 mm. Data are represented as mean ± SD. Statistical significance was based on two-way ANOVA, compared with the corresponding value of $17/H9N2^{627E}$ (ns, not significant; *, $p < 0.05$; **, $p < 0.01$; ***, $p < 0.001$).

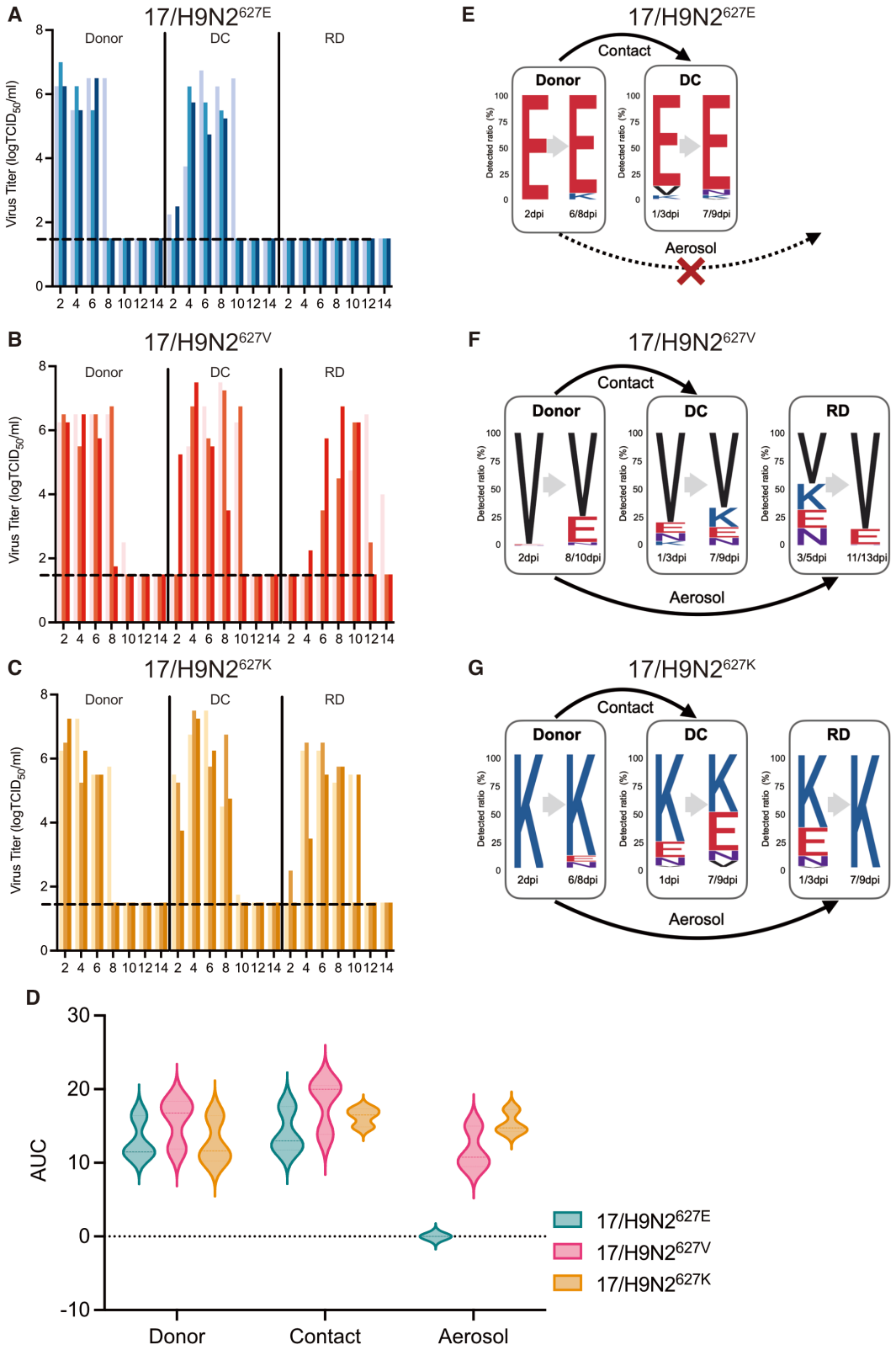
A
17/H9N2627E
Donor
DC
RD
Virus Titer (logTCID50/ml)
B
17/H9N2627V
C
17/H9N2627K
D
AUC
Donor
Contact
Aerosol
17/H9N2627E
17/H9N2627V
17/H9N2627K
E
F
G
Contact
Aerosol
Detected ratio (%)
2dpi
6/8dpi
1/3dpi
7/9dpi
8/10dpi
3/5dpi
11/13dpi
1dpi

431 **Fig. 3 PB2-627V facilitated aerosol transmissibility of H9N2 virus in ferrets.** Each ferret (n =
432 3) was inoculated with 10^6 $TCID_{50}$ of indicated virus. The next day, the infected ferret was
433 individually paired by co-housing with a DC ferret; an RD-contact ferret was also housed in a wire
434 frame cage adjacent to the infected ferret. Nasal washes were collected for virus-shedding
435 detection every other day from all ferrets from 2 dpi. (**A-C).** Virus titers of nasal washes were
436 determined by $TCID_{50}$ assays on MDCK cells. Each color bar represents virus titers of an
437 individual ferret. Dashed lines indicate the lower limit of virus detection ($10^{1.5}$ $TCID_{50}$/ml). (**D).**
438 AUC values approximate total virus output throughout infection (mean AUC from three ferrets).
439 (**E-G).** For each infected or transmitted ferret, the nasal washes collected at the first and last virus
440 detection time were analyzed by deep sequencing. Detection time points are based on the results
441 shown in Fig. 3, A-C. The height of each letter indicates the relative ratio of amino acids at PB2-
442 627. Sequencing was performed on an Illumina NovaSeq platform.
443

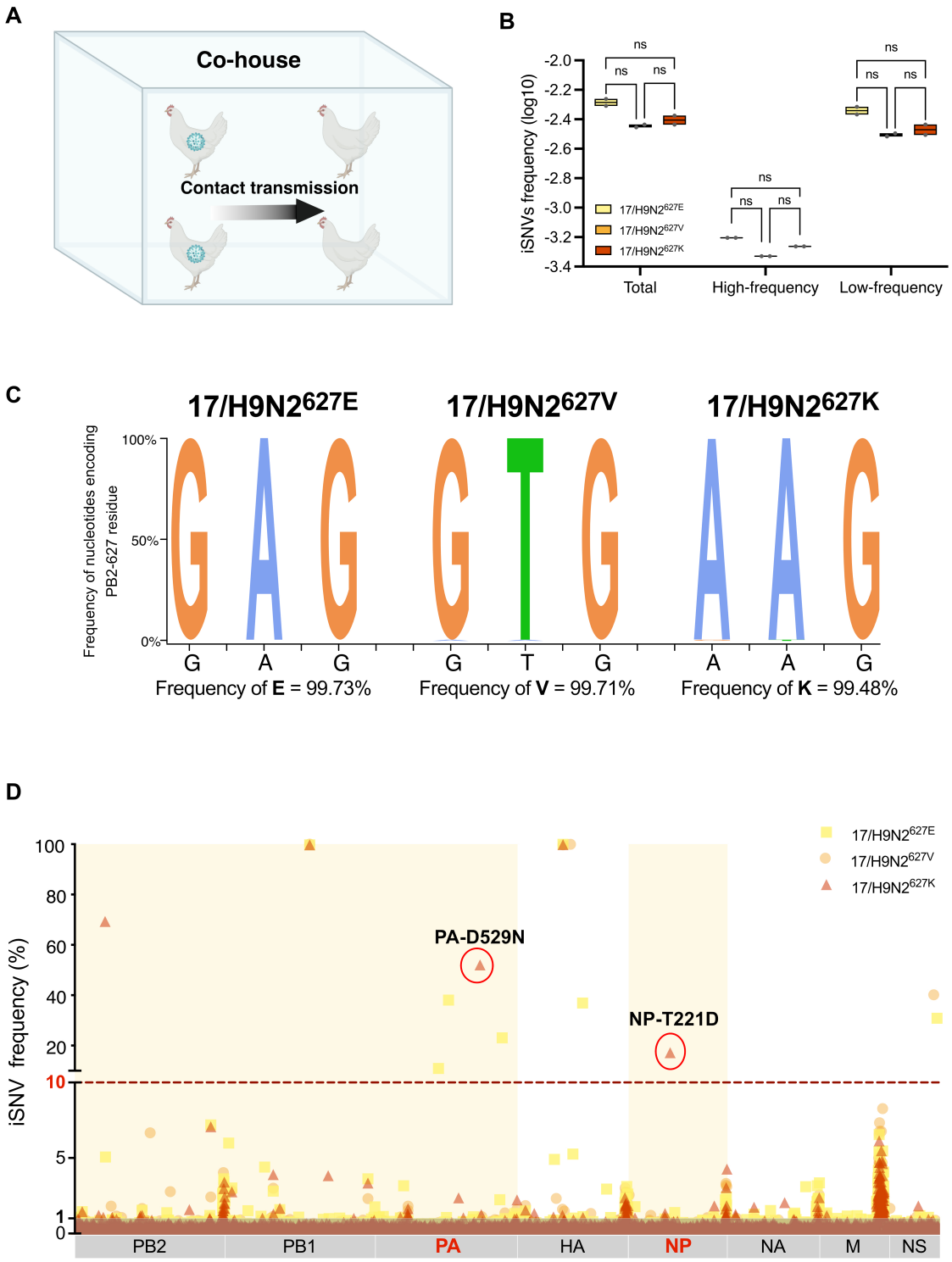

Fig. 4 PB2-627V has the potential for sustained prevalence in poultry. (A). Schematic depiction of virus passage in chickens**.** Groups of 2 chickens were each i.n. infected with 10^6 $TCID_{50}$ of indicated virus (P1), and subsequently passaged (P1-P5) by contact. **(B).** Intra-host

448 single nucleotide variants (iSNVs) frequency of P5 chicken. Variants of nucleotide site detected
449 above 1% threshold were identified as iSNVs. All iSNVs were further determined as high-
450 frequency (>10%) and low-frequency (⩽10%). iSNVs frequency of the whole genome was
451 calculated by using the number of iSNVs divided by the total number of genome sites. iSNVs
452 frequency was expressed as the log. (**C**). Variant frequency nucleotides encoding PB2-627 residue.
453 The height of each letter indicates the average ratio of nucleotides encoding PB2-627 residue in
454 two samples of each group. (**D**). Graphs represent all iSNVs detected in P5 chicken. Variant
455 frequencies are plotted by genome location and are colored by virus groups. two high-frequency
456 non-synonymous iSNVs are circled and labeled with the corresponding amino acid mutations.
457 Yellow backgrounds depict RNP genes (PB2, PB1, PA, and NP). Sequencing was performed on
458 an Illumina NovaSeq platform. Data are presented as mean ± SD. Statistical significance was based
459 on two-way ANOVA (ns, not significant, *, $p < 0.05$; **, $p < 0.01$; ***, $p < 0.001$).
460

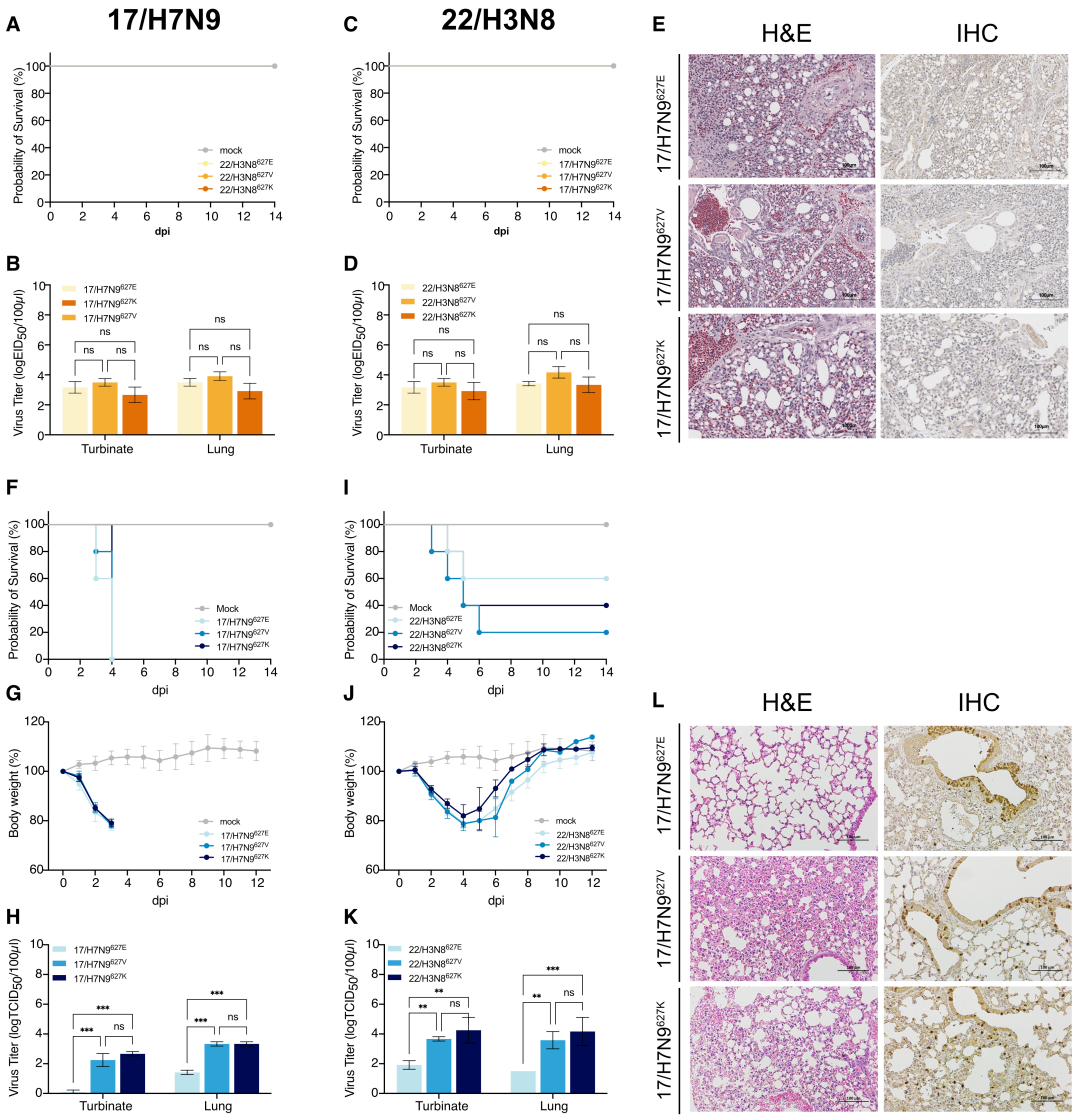

Fig. 5 PB2-627V conferred dual adaptability in avian H7N9 and H3N8 viruses to replicate in chickens and mice. (A-E). Groups of 6 chickens were infected with indicated viruses at doses of 10^6 EID_{50}. Three infected chickens in each group were monitored for survival (**A**, **C**) over 14 days. At 3 dpi, the other three chickens in each group were euthanized. Virus titers (**B**, **D**) in the turbinates and lungs were determined by $TCID_{50}$ assays. Representative histopathological findings (**E**) in the lungs of infected mice. Lung sections were stained with H&E (left) and by IHC against influenza viral NP antigen (right). Scale bars, 100 mm. **(F-L).** Groups of 8 mice were infected with indicated viruses at doses of 10^6 $TCID_{50}$. Five mice in each group were monitored for survival (**F**, **I**) and body weight changes (**G**, **J**) over 14 days. Mortality from infection included mice euthanized at a weight loss of 25% or more. At 3 dpi, the other three mice in each group were euthanized. Virus titers (**H**, **K**) in the turbinates and lungs were determined by $TCID_{50}$ assays. Representative

473 histopathological findings (**L**) in the lungs of infected mice. Lung sections were stained with H&E
474 (left) and by IHC against influenza viral NP antigen (right). Scale bars, 100 mm. Data presented
475 are represented as mean ± SD. Statistical significance was based on two-way ANOVA (ns, not
476 significant; *, $p < 0.05$; **, $p < 0.01$; ***, $p < 0.001$).
477

Materials and Methods

Ethics statement

9 to 11-day-old specific pathogen-free (SPF) embryonated chicken eggs and all experimental animals were purchased from Boehringer Ingelheim, China. All animal research was approved by the Beijing Association for Science and Technology (approval ID SYXK, Beijing, 2020-0053) and performed in compliance with the Beijing Laboratory Animal Welfare and Ethics guidelines, as issued by the Beijing Administration Committee of Laboratory Animals, and by the China Agricultural University (CAU) Institutional Animal Care and Use Committee guidelines (ID: SKLAB-B-2010-003) approved by the Animal Welfare Committee of CAU. The H9N2, H7N9, and H3N8 wild-type viruses used are all low pathogenic avian influenza (LPAI) viruses isolated from chickens. PB2-E627V and PB2-E627K are natural mutations found in these viruses.

Sequence collection and alignment

The sequences of the PB2 gene were obtained from the GISAID database (http://www.gisaid.org). After removing the PB2 sequences of human H3N2 and H1N1pdm09 viruses and duplicate sequences, a total of 42,297 full-length PB2 sequences of IAVs published globally from 1994 to 2022 were obtained. All accession codes of public sequences can be found in Dataset S1. Sequences were aligned using MUSCLE v3.7 [46] via the CIPRES Science Gateway [47].

Phylogenetic analyses

The phylogenetic tree of the H9N2 PB2 gene was constructed using a total of 4523 PB2 sequences from H9N2 subtype IAVs. The phylogenetic tree of PB2-627V was constructed using a total of 394 PB2 sequences carrying the PB2-627V. IQ-TREE version 1.6 was used to construct the maximum likelihood phylogenetic trees, applying the best-fit general time-reversible model of nucleotide substitution with gamma-distributed rate variation among sites (GTR + I + G), and performing ultrafast bootstrap resampling analysis (1000 replications). Phylogenetic trees were visualized and annotated using FigTree version 1.4.4, Adobe Illustrator 2021, and Interactive Tree Of Life (iTOL) [48].

Host transmission dynamics analyses

A maximum clade credibility (MCC) tree was performed on the PB2-627V cluster sequences (Fig. S1A) with BEAST v1.10.4. Using the coalescent Bayesian Skygrid model, the General Time Reversible (GTR) model of evolution and the strict clock were employed. The host jump patterns were interfered by mapping the host types onto the time-scaled tree using an asymmetric discrete trait model [49]. A Markov Monte Carlo (MCMC) chain is run for 30 million, sampled every 3000

511 and the first 10% of tree was removed as burn-in. Stationarity and mixing were checked with
512 Tracer v1.7.2. The MCC tree was finally generated by TreeAnnotator and visualized using FigTree
513 v1.4.4.

514 **PB2 protein structure simulation**

515 A simulation of the A/chicken/Hebei/m0530-1/2017 (17/H9N2) PB2 protein structure was
516 performed by using Swiss-Model (https://swissmodel.expasy.org). The 17/H9N2 PB2 protein
517 sequence was inputted in FASTA format, and the published H7N9 protein structure (PDB: 7qtl.1.C)
518 with 98.94% sequence identity was utilized as the template. The quality of the resulting model was
519 evaluated using GMQE and QMEAN scores. PyMOL was utilized to introduce the PB2-E627V
520 and PB2-E627K mutations into the model and to ascertain the surface charge of the protein.

521 **Cell lines**

522 Human lung epithelial cell (A549) cells, kidney epithelial (293T) cells, chicken fibroblast
523 (DF-1) cells, and Madin-Darby Canine Kidney (MDCK) cells were maintained in our laboratory.
524 Chick embryo fibroblast (CEF) cells were obtained from SPF embryonated chicken eggs as
525 previously described [50]. 293T cell line with a double knockout of ANP32A and ANP32B (DKO
526 cell) was kindly provided by Xiaojun Wang from Harbin Veterinary Research Institute. Cells were
527 cultured with Dulbecco's modified Eagle medium (DMEM; Gibco, New York, USA)
528 supplemented with 10% fetal bovine serum (FBS; Gibco, Sydney, Australia) and 1% penicillin-
529 streptomycin solution (MACGENE, Beijing, China).

530 **Influenza viruses**

531 H9N2 AIV A/chicken/Hebei/m0530-1/2017 (17/H9N2) was characterized and maintained in
532 our laboratory. Influenza H7N9 virus A/chicken/China/0606-12/2017 (17/H7N9) and influenza
533 H3N8 virus A/chicken/Shandong/FE12/2022(H3N8) (22/H3N8) were isolated by our laboratory.
534 Viruses were propagated in 9 to 11-day-old SPF embryonated chicken eggs at 35°C for 72 hours.
535 Virus titers were determined by 50% tissue culture infectious dose ($TCID_{50}$) on MDCK cells or
536 50% egg infectious dose (EID_{50}) on SPF chicken eggs.

537 **Animals**

538 5 to 6 weeks-old female SPF BALB/c mice and 6 to 8 weeks-old female SPF chickens were
539 purchased from Vital River Laboratory Animal Technology Co., Ltd (Beijing, China). Mice were
540 kept in individually ventilated cages (IVC), and chickens were kept in high efficiency particulate
541 air (HEPA)-filter isolators in the Animal Care Facilities at CAU. Five to six-month-old male
542 Angora ferrets (*Mustela putorius furo*), serologically negative for currently circulating influenza
543 viruses (H1, H3, H5, H7, and H9) and > 1.0 kg (ranging from 1.10 to 1.80 kg) in weight, were

544 purchased from Angora LTD (Jiangsu, China). All ferrets were housed in wire cages placed inside
545 HEPA-filter isolators. All animals were allowed free access to water and a standard chow diet, and
546 provided with a 12-hour light and dark cycle (temperature: 20-25°C, humidity: 40%-70%). All
547 animals used were not involved in any other experimental procedure.

548 **Generation of viruses by reverse genetics**

549 As described previously [18], recombinant viruses were generated using a plasmid-based
550 reverse genetics system in the genetic background of 17/H9N2, 17/H7N9, and 22/H3N8.
551 Mutations were introduced into the plasmids using PCR-based site-directed mutagenesis. To check
552 for the absence of unintended mutations, all propagated viruses were subjected to complete
553 sequencing.

554 **Polymerase activity assay**

555 To compare the polymerase activities of different viral ribonucleoprotein (RNP) complexes,
556 a dual-luciferase reporter assay system (Promega, Madison, WI, USA) was employed [25]. The PB2,
557 PB1, PA, and NP gene segments of respective viruses were individually cloned into the pCDNA3.1
558 expression plasmid. 125 ng of each of the PB2, PB1, PA, and NP plasmids, as well as 10 ng of the
559 pLuci luciferase reporter plasmid and 2.5 ng of the Raniera internal control plasmid, were
560 transfected into 293T cells or DF-1 cells. The cell cultures were then incubated at 33°C or 37°C
561 for 24 hours. The transfected cells were then lysed and analyzed for firefly and renilla luciferase
562 activities using a GloMax 96 microplate luminometer (Promega). The function of ANP32 was
563 examined using a polymerase assay by co-transfection of DKO cells with different ANP32 proteins
564 or empty vector (20 ng) at 33°C or 37°C for 24 hours. All of the experiments were performed
565 independently at least three times.

566 **Growth kinetics of viruses in A549 and CEF cells**

567 A549 and CEF cells were cultured in 6-well plates and infected in triplicate with indicated
568 viruses at a multiplicity of infection (MOI) of 0.1 (A549) or 0.01 (CEF). After a 2-hour incubation,
569 cells were washed three times with DPBS, and incubated at 37°C in 5% CO_2. Supernatants were
570 collected at 12, 24, 36, 48, and 60 hours post-infection (hpi), and virus titers were determined by
571 $TCID_{50}$ assays on MDCK cells.

572 **Quantitative real-time PCR assay**

573 Levels of mRNA and viral RNA (vRNA) were determined in A549 cells and DF-1 cells
574 infected in triplicate with viruses (17/H9N2^{627E}, 17/H9N2^{627V}, or 17/H9N2^{627K}) at an MOI of
575 0.1(A549 cells) or MOI of 0.001 (DF-1 cells). Total RNA was extracted from infected cells by
576 using TRIzol reagent according to the manufacturer's instructions (Invitrogen). For the detection

577 of mRNA and vRNA, the oligo(dT) primer and primer uni-12 (5'- AGCAAAAGCAGG -3') were
578 used respectively to generate cDNAs from 1 μg of total RNA per sample by using Superscript III
579 first-strand synthesis supermix (Invitrogen). The quantitative real-time PCR (qRT-PCR) mixture
580 for each reaction sample consisted of 10 μL of 2× SYBR green PCR master mix (Applied
581 Biosystems), 7 μL of nuclease-free water, 0.5 μL of each primer, and 2 μL of the cDNA template.
582 qPCR was conducted using a 7500 real-time PCR system (Applied Biosystems) with the following
583 program: 1 cycle at 95°C for 10 min, followed by 40 cycles of 95°C for 15 s and 60°C for 1 min.
584 Expression values for each gene, relative to *β-actin*, were calculated by using the $2^{-\Delta\Delta CT}$ method.
585 Each qPCR sample contained three technical replicates. Primers for the amplification of the *β-*
586 *actin* and PB2 genes are as follows: forward primer 5'-AGAGCTACGAGCTGCCTGAC-3' and
587 reverse primer 5'-CGTGGATGCCACAGGACT-3' for *β-actin*, forward primer 5'-
588 GGAACAGGAATGGACCGACA-3' and reverse primer 5'-ACTGAGATCTGCATGACCCG-3'
589 for PB2.

590 **Mouse challenge studies**

591 Groups of eight mice were anesthetized by intramuscular injection of Zoletil 50 (Zoletil;
592 Virbac SA, Carros, France) at a dose of 20 mg/kg, and inoculated intranasally (i.n.) with 10^6
593 $TCID_{50}$ of test virus or PBS in a total volume of 50 μL. At 3 days post-infection (dpi), 3 mice from
594 each group were euthanized, and lung and nasal turbinate tissues were collected for virus titration
595 in MDCK cells by $TCID_{50}$ assay. Lungs of mice infected with the indicated viruses at 3 dpi were
596 collected for histopathology and immunohistochemistry (IHC). The remaining 5 animals were
597 monitored in the remaining two weeks for disease progression, weight change, and mortality. Mice
598 that experienced a weight loss exceeding 25% of their original weight were humanely euthanized.

599 **Chicken challenge studies**

600 Experimental procedures for virus infection of chickens were under previously described
601 protocol [51]. Groups of 6 chickens were inoculated i.n. with 10^6 EID_{50} of indicated virus or PBS in
602 a volume of 200 μL. At 3 dpi, 3 chickens from each group were euthanized, and lung and nasal
603 turbinate tissues were collected for virus titration by EID_{50} assay. Lungs of chickens at 3 dpi were
604 collected for histopathology and IHC. The remaining 3 chickens were monitored and tracheal
605 swabs were taken at 2, 4, 6, and 8 dpi for virus titration by EID_{50} assay.

606 **Histopathology and IHC analysis**

607 Lungs were fixed in 10% buffered formalin, embedded in paraffin, sectioned and stained with
608 hematoxylin and eosin (H&E). Tissue sections were also immunostained with a viral NP
609 monoclonal primary antibody (ab20343, Abcam, Beijing, China). The secondary antibody used
610 was conjugated to horse radish peroxidase (HRP), and the color reaction was based on the use of

611 an HRP reaction kit (ZSGB-BIO, Beijing, China). Histopathological examination was conducted
612 blind by two experienced experimental pathologists.

613 **Virus passage in chickens**

614 For virus passage in chickens, as depicted in Fig. 4A, groups of 2 SPF chickens were
615 inoculated at passage 1 (P1) with 10^6 EID_{50} of the indicated virus in a volume of 200 μL. At 3 dpi,
616 2 naïve chickens were co-housed with the P1 chickens to establish the P2 generation. At 6 dpi of
617 P1 chickens, lung tissues of P1 chickens were collected and homogenized in 500 μL of cold PBS,
618 and another 2 naïve chickens were introduced as P3. The same sequential steps were used for
619 passage up to the P5.

620 **Ferret transmission experiments**

621 The transmission study consisted of groups of 3 ferrets, following a previously described
622 protocol[32,52] comprising one infected, one direct contact (DC), and one respiratory droplet contact
623 (RD) group. Ferrets were housed in wire cages inside isolators, with each isolator approximately
624 15 cubic feet in size. Each ferret was sedated with ketamine (20 mg/kg) and xylazine (1 mg/kg)
625 via intramuscular injection and inoculated intranasally with 10^6 $TCID_{50}$ of 17/H9N2^{627E},
626 17/H9N2^{627V}, or 17/H9N2^{627K} virus in a volume of 500 μL delivered at 250 μL per nostril. Twenty-
627 four hours later, 2 naïve ferrets were introduced into the isolator, with the direct contact ferret
628 placed in the same cage as the infected ferret, while the respiratory droplet contact ferret was
629 placed in a cage separated by a wire mesh wall to prevent physical contact.

630 Individual weight was monitored throughout the study. Nasal washes were collected from the
631 ferrets by 2 mL virus transport medium every other day for 14 days and titrated for viruses in
632 MDCK cells by TCID50 assays. Additionally, 200 μL nasal washes were used for RNA extraction
633 and deep sequencing. At 21 dpi, blood samples of ferrets were collected to determine
634 seroconversion using the HI Assay.

635 **Next generation sequencing**

636 A total of 54 ferret nasal wash samples, 6 chicken lung samples, and 3 viruses (17/H9N2^{627E},
637 17/H9N2^{627V}, and 17/H9N2^{627K}) were subjected to whole-genome sequencing. Viral RNA was
638 harvested from the samples by using the QIAamp Viral RNA Mini Kit (Qiagen). Multiplex reverse
639 transcription-PCR amplification of all 8 influenza virus genome segments was performed on RNA
640 samples using PrimeScript™ II 1st Strand cDNA Synthesis Kit (Takara 6210) and primers
641 Uni12/Inf1 (5'-GGGGGGAGCAAAAGCAGG-3'), Uni12/Inf3 (5'-
642 GGGGGAGCGAAAGCAGG-3'), and Uni13/Inf1 (5'CGGGTTATTAGTAGAAACAAGG-3').
643 As previously described [32], PCR products were purified on spin columns and quantified by using
644 the Quant-It Pico Green kit (Invitrogen, Carlsbad, USA). The purified amplicons were pooled in

645 equimolar and paired-end sequenced (23150) on an Illumina NovaSeq platform according to the
646 standard protocols. Sequencers by 200 or 250 bp paired-end sequencing, and sequencing depth for
647 avian influenza virus isolates was about 0.2 G per sample. NGS findings were validated by qRT-
648 PCR. Raw NGS reads were processed by filtering out low-quality reads (eight bases with quality
649 < 66), adapter-contaminated reads (with > 15 bp matched to the adapter sequence), poly-Ns (with
650 8 Ns), duplication and host-contaminated reads (SOAP2 [version 2.21]; less than five mismatches).
651 Sanger sequences of parental viruses were chosen as reference sequences. Burrows-Wheeler
652 Alignment Tool (version 0.7.12) and SAMtools (version 1.4) were then used to perform reference-
653 based assembly. Data analyses were performed using a custom quality-based variant detection
654 pipeline.
655 To detect the genomic variants, the iSNVs were identified as following standards: 1) reads >
656 1000; 2) mutation rates >1%. The iSNVs frequency was calculated by using the number of iSNVs
657 divided by the total number of genome sites.

658 **Quantification and statistical analysis**

659 Graphing and statistical analyses were performed using GraphPad Prism 8 (GraphPad
660 Software, San Diego, California, USA; www.graphpad.com). Experimental groups were
661 statistically compared by analysis of variance (ANOVA). P value < 0.05 was considered to indicate
662 statistical significance.

663